iScience

CellPress
OPEN ACCESS

Article

Involvement of neuronal tachykinin-like receptor at 86C in *Drosophila* disc repair via regulation of kynurenine metabolism

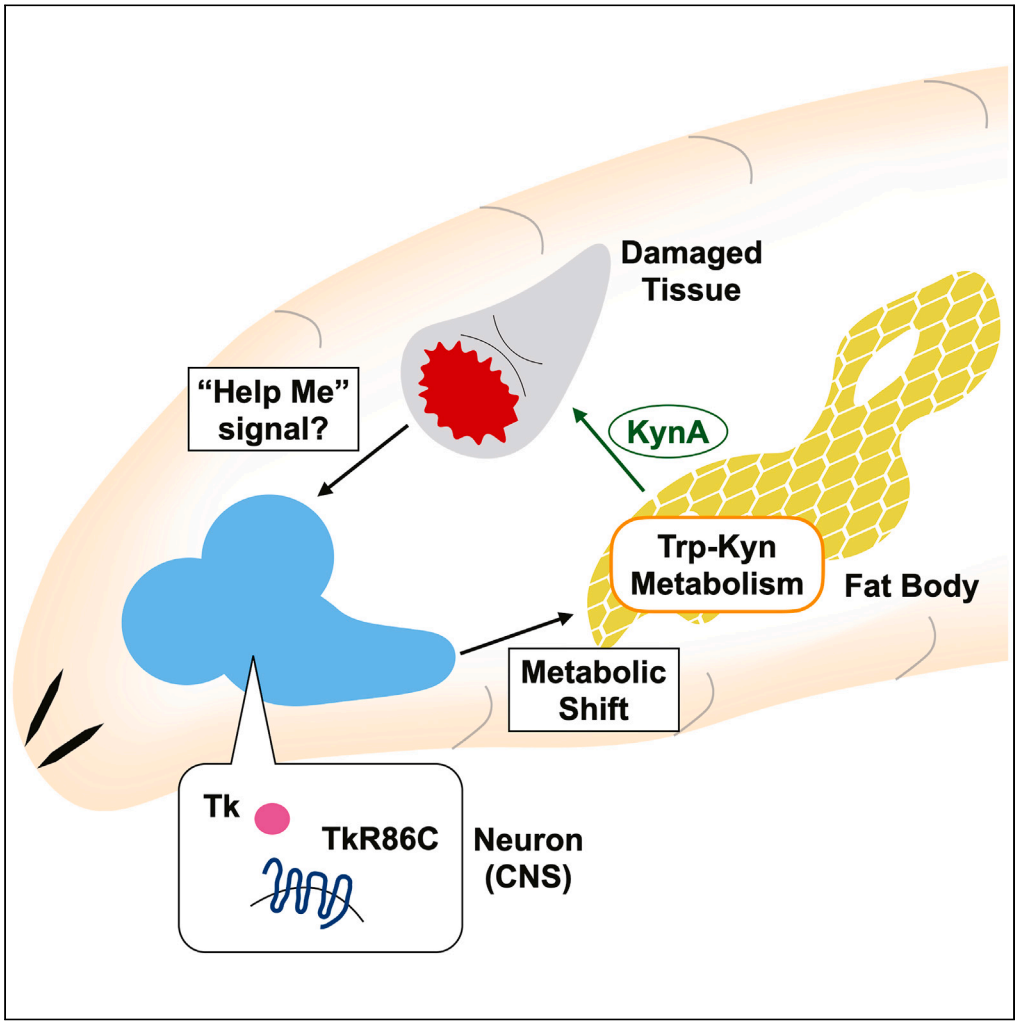

Soshiro Kashio,
Shu Masuda,
Masayuki Miura

fkashio@g.ecc.u-tokyo.ac.jp (S.K.)
miura@mol.f.u-tokyo.ac.jp (M.M.)

Highlights

Neuronal TkR86C is remotely required for *Drosophila* wing disc repair

TkR86C-RNAi in neuron remotely impairs injury-induced Kyn metabolic changes

KynA treatment recovers the wing phenotype induced by neuronal knockdown of *TkR86C*

Kashio et al., iScience *26*, 107553
September 15, 2023
https://doi.org/10.1016/j.isci.2023.107553

iScience

CellPress
OPEN ACCESS

Article

Involvement of neuronal tachykinin-like receptor at 86C in *Drosophila* disc repair via regulation of kynurenine metabolism

Soshiro Kashio,[1,2,*] Shu Masuda,[1,2] and Masayuki Miura[1,3,*]

SUMMARY

Neurons contribute to the regeneration of projected tissues; however, it remains unclear whether they are involved in the non-innervated tissue regeneration. Herein, we showed that a neuronal tachykinin-like receptor at 86C (TkR86C) is required for the repair of non-innervated wing discs in *Drosophila*. Using a genetic tissue repair system in *Drosophila* larvae, we performed genetic screening for G protein-coupled receptors to search for signal mediatory systems for remote tissue repair. An evolutionarily conserved neuroinflammatory receptor, TkR86C, was identified as the candidate receptor. Neuron-specific knockdown of *TkR 86C* impaired disc repair without affecting normal development. We investigated the humoral metabolites of the kynurenine (Kyn) pathway regulated in the fat body because of their role as tissue repair-mediating factors. Neuronal knockdown of *TkR86C* hampered injury-dependent changes in the expression of *vermillion* in the fat body and humoral Kyn metabolites. Our data indicate the involvement of TkR86C neurons upstream of Kyn metabolism in non-autonomous tissue regeneration.

INTRODUCTION

Tissue repair is a harmonious system based on cell-to-cell and tissue-to-tissue interactions. Recognition of and response to the surrounding environment of cells is essential. One example is when apoptotic cells in damaged sites send signals to the surrounding cells. In the case of head regeneration of the hydra, the morphogen Wnt3, secreted from apoptotic cells, promotes the proliferation of stem or interstitial progenitor cells.[1] The contribution of apoptotic cells to cell proliferation has been revealed in the mouse liver and *Drosophila* imaginal discs (larval epithelial tissues determined to be adult tissues).[2–5] Moreover, the interactions among different types of cells or tissues are indispensable for tissue repair. In newt and axolotl limb regeneration, factors secreted from peripheral nerves near the amputated limbs, such as neuregulin, fibroblast growth factors, and bone morphogenetic proteins, are required for blastema formation.[6,7] The proliferative factors oncostatin M or PDGF-AA from Schwann cell precursors in mice are essential for the proliferation of mesenchymal cells and subsequent digit regeneration.[8] In addition, the wound epithelia in amputated axolotl limbs secrete MARCKS-like proteins that trigger the proliferation of blastema.[9]

Tissue damage responses are not locally restricted; remote tissues also respond to local tissue damage, known as the systemic damage response or systemic wound response.[10,11] Recent studies have revealed the non-autonomous effects of remote tissues on regeneration. Our previous studies have indicated that imaginal disc repair is supported by the fat body in *Drosophila* larvae. The invertebrate fat body is the functional counterpart of the mammalian liver and white adipose tissue, which are metabolically active secretory tissues. We found that the metabolism of methionine-S-adenosylmethionine (Met-SAM) and tryptophan-kynurenine (Trp-Kyn) in the fat body remotely regulates disc repair.[12,13] This indicates that interactions between damaged and distant tissues are essential for tissue repair; however, the tissues required for imaginal disc repair cannot be restricted to the fat body. Additionally, signal interactions between distant tissues for tissue repair are largely unknown.

As mentioned previously, neurons contribute to the regeneration of surrounding tissue, but innervation is not observed in wing discs until the pupal stage.[14] The involvement of the nervous system in tissue regeneration without direct neural projections has not yet been examined. To reveal the neuroprojection-independent

[1]Department of Genetics, Graduate School of Pharmaceutical Sciences, University of Tokyo, 7-3-1 Hongo, Bunkyo-ku, Tokyo 113-0033, Japan

[2]These authors contributed equally

[3]Lead contact

*Correspondence: fkashio@g.ecc.u-tokyo.ac.jp (S.K.), miura@mol.f.u-tokyo.ac.jp (M.M.)

https://doi.org/10.1016/j.isci.2023.107553

aspects of tissue repair/regeneration between neurons and wing discs, we performed a functional analysis of receptors, especially G protein-coupled receptors (GPCRs). The GPCR family is the largest family of receptors and a wide range of ligands, including small molecules, peptides, and lipids.[15] However, comprehensive analyses of GPCRs have not been performed in the context of regeneration. We exploited the genetic tissue repair system in *Drosophila* and performed RNAi screening of GPCRs for imaginal disc repair. From this genetic screening, we found that the tachykinin-like receptor at 86C (TkR86C) in neurons and its ligand, tachykinin (Tk), were required for disc repair, while impairment of this pathway did not affect normal development. Additionally, neuronal knockdown of *TkR86C* affects Kyn metabolism in the fat body and Kyn metabolites in the hemolymph, influencing remote disc repair.

Herein, we report that the involvement of TkR86C and ligand-expressing neurons in tissue repair brings new insights into tachykinin-based tissue repair functions and tissue interactions for tissue repair.

RESULTS

GPCR screening identifies TkR86C as a candidate receptor for disc repair

Drosophila larvae have regenerative epithelial tissues, wing imaginal discs, in which the wing pouch (WP) region is determined to be an adult wing; thus, we can examine the extent of tissue repair by observing the wing phenotype.[16,17] We have previously established a WP region-specific cell ablation and repair system using a temperature-sensitive form of the diphtheria toxin A domain (DtA^{ts}).[12] By inducing DtA^{ts} cell ablation using the *WP-QF2* driver and a temporal temperature shift, we independently manipulated gene expression using the Gal4 driver (Figure 1A). To identify new tissue interactions, we manipulated GPCR genes in the repairing wing discs using a pan disc Gal4 driver, *C10-Gal4* driver, which is mainly expressed in the entire imaginal discs, salivary glands, parts of the central nervous system (CNS), and parts of the gut, but not in the fat body (Figures S1A–S1E′; Table S2).

Among the 106 GPCR genes (excluding olfactory receptors, listed based on FlyBase), 10 were selected as candidate genes (Figure 1B; Table S1). We focused on TkR86C for further studies because the two distinct RNAi lines reproducibly produced defective wing phenotypes (Figure 1C). *Drosophila* has two tachykinin receptor orthologs: TkR86C and the tachykinin-like receptor at 99D (TkR99D).[18] Although TkR99D is involved in lipid accumulation in the gut and nociceptive responses in neurons,[19,20] TkR86C has been reported to be involved in aggressive male behavior and daily locomotor activity.[21,22] However, there are no reports on the function of TkRs in *Drosophila* tissue repair or regeneration.

In addition to the wing phenotype, disc morphologies were examined with the morphogen wingless (Wg), which expresses a ring-like shape pattern in the WP region and dorsal-ventral boundary and is required for wing development. Immediately after DtA^{ts} cell ablation (0h after ablation; AA0), the Wg signal became sparse and decreased in intensity (Figures 1E and 1F). After 12 and 24 h of ablation (AA12 and AA24), the recovered wing discs showed a ring-like pattern of Wg (Figures 1E′ and 1E″). On the other hand, in *TkR86C* knocked down larvae, wing discs showed an abnormal pattern of Wg expression (Figures 1F′ and 1F″). Importantly, without disc injury, *TkR86C-RNAi* did not affect normal wing development, developmental speed (Figures 1D and 1G), or damage-dependent developmental delay (Figure 1H), indicating that TkR86C contributes to disc repair without affecting developmental delay or wing development.

TkR86C is highly expressed in the central nervous system, and neuron-specific repression of TkR86C results in disc repair defects

To determine the site where TkR86C functions, we examined the expression pattern of *TkR86C* with *TkR86C-T2A-Gal4* and *TkR86C-T2A-LexA* drivers, which allows us to determine the endogenous expression patterns under Gal4 or LexA drivers with the self-cleaving peptide T2A.[23,24] The *TkR86C-T2A-LexA* driver showed strong expression in the brain and ventral nerve cord (Figures S2A and S2A′). As for wing discs, *TkR86C* expression was induced in a small part of the cell cluster at the WP and hinge or pleura region of damaged discs and was slightly observed in non-damaged wing discs (Figures S2C and S2D). A previous study reported that hemocytes were recruited to damaged discs,[25] but *TkR86C* positive cells were not marked by the hemocyte marker P1[26] (Figures S2E–S2E″), suggesting that *TkR86C* is expressed in damaged disc cells.

To investigate the involvement of induced *TkR86C* in wing discs, *TkR86C* was knocked down using a pouch expressing *rn-Gal4* driver (Figure S3). The *rn-Gal4* driver could cover TkR86C induced in the

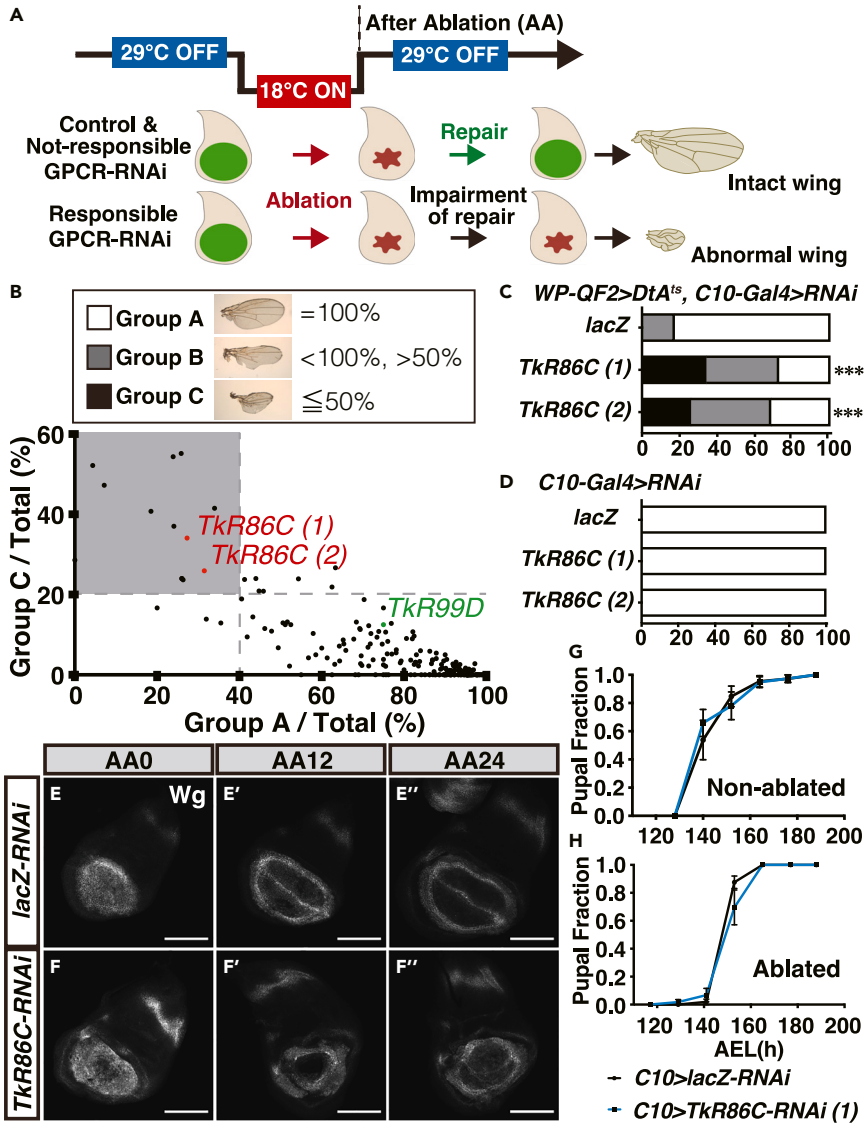

Figure 1. TkR86C as a candidate receptor for disc repair, identified using GPCR screening

(A) Scheme of disc repair and screening. DtA^{ts}-dependent cell ablation is induced by a temperature shift from the early to middle 3rd larval stage. While tissue repair occurs after ablation under normal conditions, it is impaired by the knockdown of the responsible GPCRs.

(B) Results of the RNAi screening of GPCRs. Candidate genes are presented as gray areas.

(C and D) Comparison of adult wing sizes between ablated and non-ablated *C10-Gal4>TkR86C-RNAi* flies. From top to bottom, n = 92, 88, and 54, and 146, 126, and 148, respectively. Statistical analysis was conducted using the Chi-squared test to compare the control (*WP-QF2>DtA^{ts}, C10-Gal4>lacZ-RNAi*) with the treated larvae; *** $p < 0.001$. Data in (C) were selected from (B).

(E and F″) Wing discs of ablated *C10-Gal4>TkR86C-RNAi* larvae developed within the indicated time course. The discs were stained with anti-Wg antibody. White scale bar, 100 μm.

(G–H) Timing of pupation in non-ablated and ablated *C10-Gal4>TkR86C-RNAi* flies. n = 116, 88, and 43, 37, respectively. The SEM was calculated from four repeated experiments. AEL: hours after egg laying. The temperature treatment is described in the STAR methods.

WP region but not TkR86C induced in the hinge or pleura region (Figures S3A–S3A‴). Knockdown of *TkR86C* using the *rn-Gal4* driver showed a worsened wing phenotype in only one RNAi line (Figure S3B). These results suggest that induced TkR86C in the injured wing discs can affect regeneration to some extent.

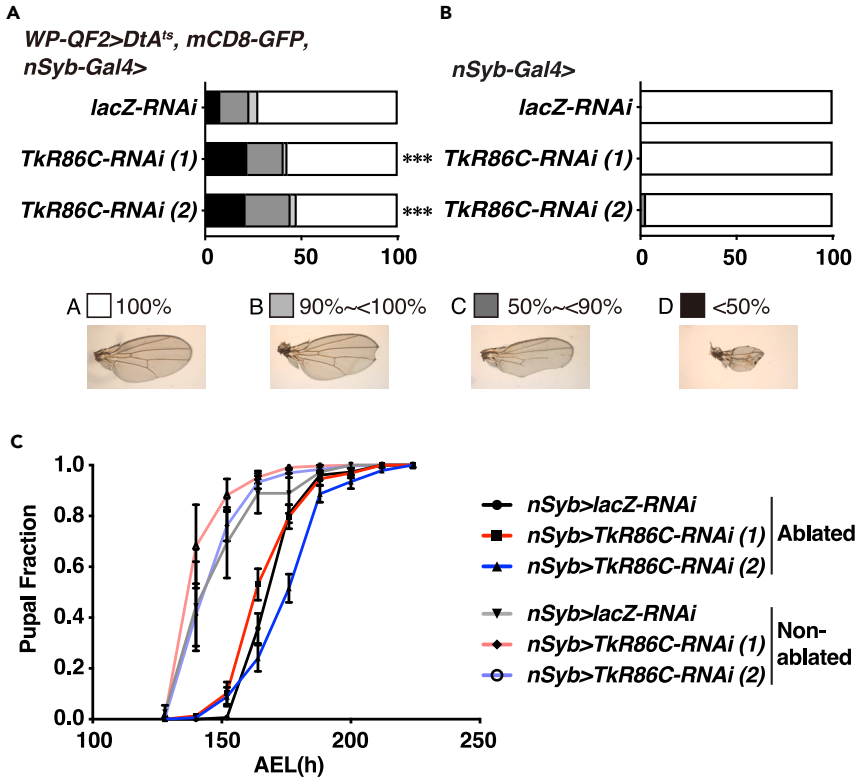

Figure 2. Neuronal TkR86C contributes to disc repair non-autonomously

(A) Comparison of adult wing sizes of ablated *nSyb-Gal4>TkR86C-RNAi* flies. From top to bottom: n = 132, 276, and 140.

(B) Comparison of adult wing sizes of non-ablated *nSyb-Gal4>TkR86C-RNAi* flies. From top to bottom: n = 192, 206, and 124. Statistical analysis was conducted using the Chi-squared test to compare the control (*WP-QF2>DtA^{ts}, nSyb-Gal4>lacZ-RNAi*) with the treated larvae; ***p < *0.001*.

(C) Timing of pupation for *nSyb-Gal4>TkR86C-RNAi* flies in ablated and non-ablated conditions. n = 108, 127, 177 and 30, 209, 162, respectively. Error bars indicated SEM. AEL: hours after egg laying. Temperature treatment is described in the STAR methods.

The *C10-Gal4* driver used for GPCR screening was strongly expressed in the CNS (Figures S1C and S2A″; Table S2). We observed neurons co-expressing *C10-Gal4* and *TkR86C-T2A-LexA* in some parts of the CNS (Figure S2B). Therefore, we considered the involvement of neuronal *TkR86C* in wing disc repair. Knockdown of *TkR86C* with pan-neuronal Gal4, a *nSyb-Gal4* driver (Figure S4), induced a worsened wing phenotype (Figure 2A). The knockdown of *TkR86C* with the *nSyb-Gal4* driver did not affect normal wing development, as seen when knocking it down using the *C10-Gal4* driver under non-disc injury conditions (Figures 2B and 1D). We confirmed that the *nSyb-Gal4* driver was not expressed in the wing disc and that neurons did not project to the wing disc but projected onto the leg disc, as previously reported[14] (Figures S4A and S4A′), indicating that *TkR86C*-expressing neurons are involved in disc repair without projection to wing discs.

Although TkR99D has been reported to be involved in nociceptive responses,[20] *TkR99D-RNAi* was not detected during the initial screening (Figure 1B; Table S1). To confirm the involvement of TkR99D, *TkR99D* was knocked down using additional RNAi lines and the *nSyb-Gal4* driver (Figure S5). Similar to the initial screening results (Figure 1B), neuronal knockdown of *TkR99D* did not worsen the wing phenotype (Figure S5), indicating that *TkR86C*-expressing neurons are specifically required for disc repair.

Disc injury causes developmental delays through an axis composed of damaged disc-derived *Drosophila* insulin-like peptide 8 (Dilp8) and Lgr3 receptor-expressing neurons that regulate ecdysone signaling.[27,28] We investigated whether the knockdown of *TkR86C* in neurons affected disc repair by regulating developmental delay. Neuronal *TkR86C* knockdown did not affect the developmental delay (Figure 2C), indicating that *TkR86C*-expressing neurons affect disc repair independent of the regulation of developmental delay.

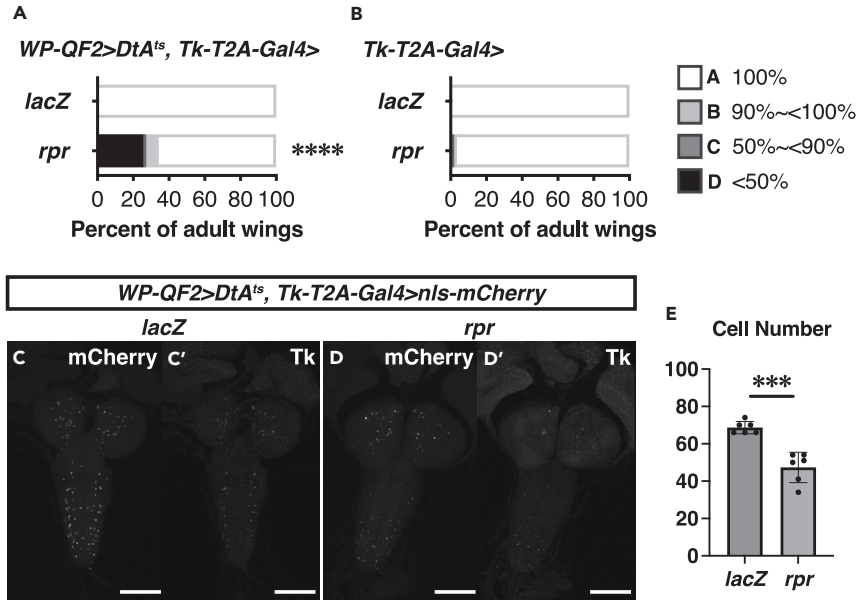

Figure 3. Ablation of *Tk*-expressing neurons impairs disc repair non-autonomously

(A and B) Comparison of adult wing sizes of *Tk*-expressing cell-ablated flies. n = 72, 68 (A); n = 82, 145 (B). Wing phenotype categories are the same as in Figure 2A. Statistical analysis was conducted using the Chi-squared test; **** $p < 0.0001$.

(C–D′) Expression patterns of *Tk-T2A-Gal4>nls-mCherry* (C, D) and signals of Tk antibody staining (C′, D′) with or without *rpr* ablation in CNS at AA24. White scale bar: 100 μm.

(E) Quantified data of cell number of *Tk-T2A-Gal4>nls-mCherry*-expressing cells in CNS (C, D). SEM was calculated from six independent samples. The two-tailed Student's *t* test was applied; *** $p < 0.001$.

TkR86C ligand tachykinin-expressing cells are required for non-autonomous disc repair

To confirm the involvement of TkR86C in disc repair, we established *TkR86C* null mutant and examined its gene expression and wing phenotype. Defects in *TkR86C* expression were confirmed in the null mutant (Figure S6A); however, the *TkR86C* null mutant did not worsen or showed a slightly better wing phenotype (Figures S6B and S2A). One possible reason for the different phenotypes in *TkR86C* mutants and RNAi could be a compensatory network that buffers against harmful mutations, as previously discussed.[29]

To verify that the RNAi phenotype was not off-target, we knocked down *TkR86C* in *TkR86C* mutant larvae. In *TkR86C* mutant larvae, *TkR86C* knockdown did not worsen the wing phenotype (Figure S6C), supporting a compensatory network to buffer the phenotype in *TkR86C* mutants at the systemic level, whereas neuron-specific knockdown of *TkR86C* resulted in a regeneration defect phenotype.

To confirm that TkR86C signaling in neurons contributes to disc repair, we investigated its ligands. TkR86C is associated with natalisin (NTL) and Tk ligands.[18] In particular, NTL-1–5 and Tk-6 showed higher binding capacities to TkR86C than to other neuropeptides.[30,31] We first checked the expression patterns of Tks to determine their sources. *Tk-T2A-Gal4* showed strong expression in the CNS (Figures S7A–S7C′). Given the restricted expression of Tk compared with that of TkR86C (Figures S7 and S2), ligand-expressing cells were ablated with an apoptosis-inducing gene, *reaper* (*rpr*), which worsened the wing phenotype after wing disc injury (Figures 3A and 3B). In addition, the fact that the wing phenotype in control lines is less severe when using *Tk-T2A-Gal4* than *C10-Gal4* or *nSyb-Gal4* (Figures 1C and 2A) may be due to the influence of different genetic backgrounds depending on the recombinant Gal4 drivers as in our previous studies.[12,13] Tk expression in the CNS was confirmed by mCherry signals and Tk antibody staining. mCherry signals induced by *Tk-T2A-Gal4* co-localized with Tk antibody signals and were detected more sensitively than Tk antibody, confirming the reduction of *Tk*-expressing cells in the CNS by *rpr*-ablation (Figures 3C–3E). Tk expression was not observed in wing discs (Figure S7C), so Tk was also required for non-autonomous disc repair. Additionally, the knockdown of *Tk* in the whole body using the *da-Gal4* driver worsened the wing phenotype (Figure S8A), supporting the involvement of Tk in non-autonomous disc repair. Unlike Tk, NTL could not be functionally analyzed in this study for reasons such as lethality due to genetic manipulation, including RNAi. Considering the results of

neuronal knockdown of *TkR86C* with several RNAi lines and *Tk*-expressing cell ablation (Figures 2 and 3), phenotypic compensation via a different pathway occurred in mutants at the systemic level, whereas neuron-specific knockdown of *TkR86C* resulted in a regeneration defect phenotype.

To investigate the CNS response to disc injury, we first measured the gene expression levels of *TkR86C*, *TkR99D*, *NTL*, and *Tk* in the larval CNS at the early stage of disc repair (Figures S9A–S9D). None of the four genes showed changes in expression in the larval CNS with a disc injury. To verify local ligand changes, we stained the CNS with anti-Tk antibody before ablation (BA) and at 0, 12, and 24 h after ablation (AA0, 12, and 24) to quantify the signal of Tk-expressing cells in the brain and VNC (Figures S8B–S8F). As development progressed, Tk signals in the brain and VNC decreased with or without injury (Figures S8E and S8F). However, in the brain and VNC of injured larvae, the decrease in the Tk signal was suppressed after AA0 and was higher in damaged larvae than in non-damaged larvae. This suggests that local Tk levels in the CNS remain high in response to injury, contributing to TkR86C-mediated repair regulation.

To verify the positional relationship between TkR86C and Tk neurons, we examined the localization of *TkR86C*-expressing and *Tk*-expressing cells in the larval CNS (Figure S10). Additionally, since the proximity of insulin-producing cell (IPC) dendrites and *Tk*-expressing cells was observed in the adult *Drosophila* brain, and knockdown of *TkR99D* in IPC was reported to increase Dilp2 signaling in IPC,[32] we examined the localization of Dilp2-producing cells (IPC), Tk, and TkR86C in the larval brain. The TkR86C signal was broadly observed in the brain and the VNC, and the signal from some Tk neurons was adjacent to the TkR86C signal (Figures S10A and S10B; orange arrows). This supports the relationship between Tk and TkR86C neurons. Although no clear observation was made regarding the adjacency or projection of Tk and Dilp2 (Figures S10C and S10D; yellow arrow), Dilp2-producing cells colocalized with a portion of TkR86C (Figures S10C and S10D; white arrowhead). This suggests that *TkR86C*-expressing neurons can affect Dilp2 neurons, similar to TkR99D neurons.

TkR86C in neurons affects damage-induced changes in humoral kynurenine metabolites

The mechanism by which TkR86C affects disc repair in neurons remains unclear. Previously, we identified that disc injury affects Kyn and kynurenic acid (KynA) levels in the hemolymph and that these metabolic changes influence disc repair.[13] We hypothesized that TkR86C contributes to disc repair by working with Kyn metabolism (Figure 4A).

First, the binding capacities of Kyn and KynA to TkR86C were investigated. It has also been reported that Kyn or KynA bind to the orphan GPCR GPR35,[33] but a recent GPCR-binding assay did not detect the binding capacity of KynA to GPR35.[34] Therefore, whether Kyn and/or KynA target GPCRs remains unclear. We hypothesized that Kyn and/or KynA affect GPCR function as ligands or allosteric regulators. Using a binding assay with the promiscuous G-protein Gα15 and the calcium indicator Fluo-4 in HEK293T cells,[35] we confirmed that TkR86C binds to Tk-6 and NTL-5, as observed in previous studies[30,31] (Figures S11A and S11B). We investigated whether KynA or Kyn affected the binding efficiency or efficacy of TkR86C to Tk-6 or NTL-5; however, neither direct binding nor allosteric regulation of TkR86C activity by KynA or Kyn was observed (Figures S11A and S11B).

Next, we investigated Trp-Kyn metabolism in the fat body and hemolymph during disc repair (AA12) using qPCR and LC-MS/MS to determine whether TkR86C functions upstream of the damage-induced metabolic changes in the fat body and hemolymph (Figures 4B–4D).

Regarding transcriptional changes in the fat body during disc repair, the transcriptional level of *v* was higher in the disc-ablated larval fat body, as previously reported[13] (Figure 4B). However, this was not observed in the larval fat body of neuronal *TkR86C* knocked down larvae (Figure 4B). *Kyat* and *cn* showed no differences due to the injury (Figure 4B). Consistent with the transcriptional changes in *v* in the fat body, the disc-damaged larval fat body showed higher levels of Kyn and KynA at AA12, and KynA levels were impaired by neuronal *TkR86C* knockdown (Figure 4C). The reason for the higher 3-hydroxykynurenine (3-HK) levels in the fat body of injured larvae with neuron-specific *TkR86C* knockdown is unknown (Figure 4C), but it is possibly because KynA, which should increase with injury, is suppressed by *TkR86C* knockdown in neurons, leading to an increase in 3-HK production. Additionally, although Trp and 3-HK showed no difference due to injury (Figure 4D), disc-damaged larval hemolymph showed higher levels of Kyn and KynA at AA12, as previously reported[13] (Figure 4D). However, this was not observed in the neuronal *TkR86C*

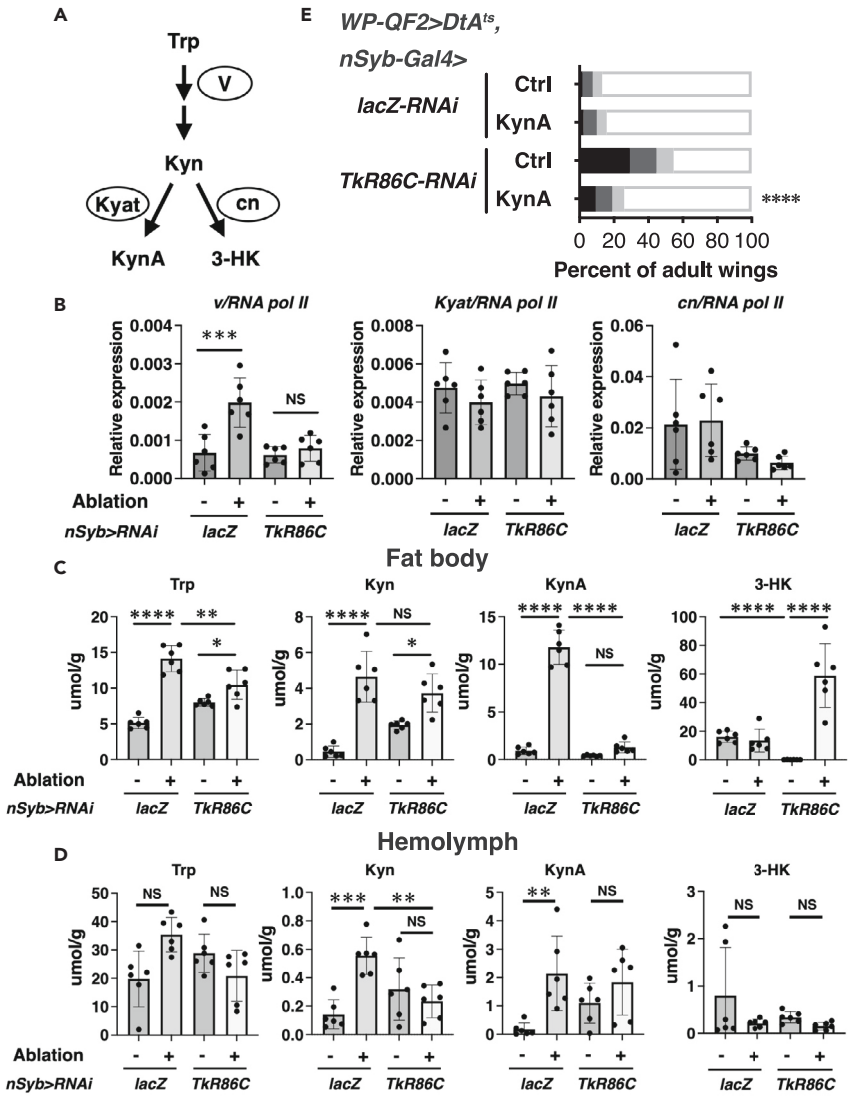

Figure 4. Neuronal knockdown of *TkR86C* hampers injury-inducing changes of kynurenine metabolites in the fat body and hemolymph during disc regeneration

(A) Schematic view of Trp-Kyn metabolism. Trp; Tryptophan, Kyn; Kynurenine, KynA; Kynurenic acid, 3-HK; 3-hydroxykynurenine.

(B) The expression levels of *v*, *Kyat*, and *cn* in the disc-ablated and non-ablated larval fat body. SEM was calculated from six independent samples. One-way ANOVA Tukey's multiple comparison test was applied: NS, not significant; **** $p < 0.0001$.

(C and D) The levels of Trp, Kyn, KynA, and 3-HK in the disc-ablated and non-ablated larval fat body (C) and hemolymph (D) with neuron-specific RNAi of *lacZ* or *TkR86 C* at AA12. The metabolites were measured using UPLC-MS/MS. SEM was calculated from six independent samples. One-way ANOVA Tukey's multiple comparison test was applied: NS, not significant; * $p < 0.05$; ** $p < 0.01$; *** $p < 0.001$; **** $p < 0.0001$.

(E) Adult wing sizes of KynA-administrated and ablated *nSyb-Gal4>TkR86C-RNAi* flies. n = 260, 210, 260, and 316, respectively. Wing phenotype categories are the same as in Figure 2A. Statistical analysis used the Chi-squared test to compare the control with KynA; **** $p < 0.0001$.

knocked down larval hemolymph (Figure 4D). Considering that the signal of *nSyb>mCD8-GFP* was not observed in the fat body (Figures S4B–S4C′), *TkR86C*-expressing neurons may affect fat body Kyn metabolism in an endocrine manner.

Kyn metabolites were also measured in the hemolymph of *TkR86C* mutant larvae, which did not show repair inhibition (Figure S6B), and no differences were observed compared with the wild type under

non-damaged condition (Figure S6D), supporting the involvement of Kyn metabolism in neuronal TkR86C-mediated disc repair. To confirm the requirement of humoral KynA for disc repair in neuronal *TkR86C*-knockdown larvae, an oral KynA-feeding experiment was conducted (Figures 4E and S12). KynA administration at AA0 recovered the severe wing phenotype of neuronal *TkR86C* knocked down larvae (Figure 4E). The wing phenotype of neuron-specific *lacZ*-RNAi adult wings was not enhanced (Figure 4E), implying that humoral KynA levels in the damaged control larvae were saturated to support disc repair, as previously observed.[13] KynA administration tended to increase the humoral KynA levels at AA12, although the difference was not significant (Figure S12). Considering that the amount of KynA in the hemolymph would have stabilized between the administration of KynA from AA0 to AA12 and that KynA levels in the damaged larval hemolymph were already higher than those in the non-damaged larval hemolymph (Figure 4D), the range of the increase in KynA levels in the hemolymph of KynA-treated larvae could explain the rescue of the wing phenotype by KynA administration (Figures S12 and S4E).

These results suggest that neuronal TkR86C affects disc repair via humoral changes in Kyn metabolite levels regulated by fat bodies (Figure S13).

DISCUSSION

The present study found that neuronal TkR86C was non-autonomously required for disc repair (Figure S13). We first searched for GPCRs that regulate regeneration using *C10-Gal4* driver expression in various tissues, including wing discs and neurons. Based on this expression pattern, we especially examined neuronal TkR86C and found that it affected disc repair non-autonomously. The interactions between damaged tissues and nerve have been investigated in mice and amphibians.[36,37] However, these studies investigated the peripheral nerves adjacent to the damaged tissue. The present study found the non-autonomous involvement of *TkR86C*-expressing neurons in non-innervated wing disc repair by utilizing a tissue-specific genetic manipulation system.

Although there are no reports on tachykinin signaling in tissue repair in *Drosophila*, mammalian tachykinins, and their receptors have been reported to affect wound responses. In particular, substance P (SP), a mammalian tachykinin, and its receptor, the neurokinin 1 receptor (NK1R), have been extensively studied. Peripheral SP and NK1R have also been reported to affect tissue repair. SP is expressed in corneal nerves, and NK1R is expressed in corneal epithelial cells and keratocytes, which support epithelial proliferation and keratocyte migration upon wounding.[38] SP expression is also induced in the tubules of injured kidneys by ischemia reperfusion and functions in tissue repair by modulating macrophages, bone marrow-derived neutrophils, and mesenchymal stromal cells.[39] However, for disc repair in *Drosophila*, Tk was not expressed in damaged discs (Figure S7C). Considering the distance between regenerating tissues and *Tk*- or *TkR86C*-expressing neurons, our findings indicate the non-autonomous regulation of tissue repair by *Tk*- or *TkR86C*-expressing neurons without direct innervation of damaged tissues.

However, the mechanisms underlying the regulation of TkR86C and Tk in disc repair remain unclear. Gene expression of *TkR86C* or *Tk* was not upregulated in the CNS after disc damage (Figure S9), whereas Tk signals marked with anti-Tk antibody were higher in the damaged larval CNS (Figures S8C–S8F); therefore, suggesting that local induction or maintenance of Tk or Tk secretion might be induced during tissue repair. Noxious stimuli induce peripheral epithelial or immune cells to release or generate multiple factors, including proteases, lipids, and purines, which cause SP secretion from peripheral neurons.[40] For example, protease allergens activate transient receptor potential $V1^+$ ($TRPV1^+$) sensory neurons to induce itching responses and SP release.[41] In addition, the endogenous α,β-unsaturated aldehyde, 4-hydroxy-2-nonenal (HNE), activates TRPA1 channels and promotes SP release from the spinal cord and peripheral nerves.[42] HNE is produced when reactive oxygen species peroxidate membrane phospholipids in response to tissue injury, inflammation, and oxidative stress. Therefore, it is possible that inflammatory factors, including damage-associated molecular patterns or reactive oxygen species from damaged discs or proteases from other inflammatory tissues, such as hemocytes and the fat body, induce Tk induction or secretion and regulate tissue repair by neurons. Additionally, a recent study indicated that Kyn released from the fat body induces the formation of zinc storage granules in Malpighian tubules, where 3-HK and the xanthurenic acid act as endogenous zinc chelators.[43] Considering that zinc is a known modulator of SP release,[44,45] humoral Kyn may also regulate Tk release through zinc homeostasis during disc repair.

However, the direct target tissues of *TkR86C*-expressing neurons and the mechanism by which *TkR86C* regulates disc repair remain unknown. However, we found that *TkR86C* knockdown in neurons repressed fat body and humoral Kyn metabolic changes during tissue repair (Figures 4C and 4D). These data imply that *TkR86C*-expressing neurons affect humoral Kyn metabolites produced in the fat body. Several *in vivo* examples of alterations in Kyn metabolism have been reported. For example, it has been reported that exercise-induced skeletal muscle PGC-1α1 modulates the production of KynA[46] and the tissue non-autonomous effect of muscle-derived KynA increases energy expenditure in adipose tissue by activating GPR35.[47] Other studies have reported that hypoxic preconditioning increases serum Kyn levels in an indoleamine 2,3-dioxygenase 1 (Ido1)-dependent manner, which is required for organ protection against ischemic kidney injury in mice.[48] The expression of Ido1 and Ido2, rate-limiting enzymes in the conversion of Trp to Kyn, is induced by interferon-gamma during inflammation.[49] As tachykinin signaling is also induced during inflammation and injury, TkR86C neuron-mediated changes in humoral Kyn metabolites suggest a new remote regulatory pathway for Kyn metabolic changes during inflammation and injury *in vivo*.

The *TkR86C* null mutant did not show a wing phenotype, unlike the *TkR86C* knockdown (Figures S6B and S2A). One possible reason for the different phenotypes of *TkR86C* mutants and RNAi could be a compensatory network that buffers harmful mutations.[29] In zebrafish, as well as in mice and *Arabidopsis*, it has become clear that there are significant differences between the phenotypes caused by gene mutation and those caused by gene knockdown. For example, zebrafish *egfl7* mutants, an endothelial extracellular matrix gene, show no obvious phenotype, whereas animals injected with *egfl7* morpholino show severe vascular defects.[50] This is because other extracellular matrix factors were increased in the mutants to compensate for the loss of *efgl7*. Considering these observations, it is implied that although neuron-specific knockdown results in an inhibitory regeneration phenotype, phenotypic compensation via a different pathway may occur in the *TkR86C* mutant during disc repair.

Elucidation of the interactions between the CNS and fat body are important for future understanding of the regulation of Kyn metabolites by TkR86C neurons. Regarding secretory signals from the fat body to the CNS, various molecular mechanisms have been reported in which the fat body senses the nutritional status, such as amino acids and carbohydrates, and regulates it by controlling the CNS.[51] For example, the leptin-like cytokine Upd-2 from the fat body relieves the inhibitory tone of GABAergic neurons that project to IPCs, resulting in Dilp secretion.[52] Eiger, a tumor necrosis factor alpha ortholog, is secreted from fat bodies under low-protein dietary conditions and inhibits Dilp production in IPCs.[53] Although secretory signals from the CNS to the fat body are less well understood than fat body-derived signals to the CNS, in the context of injury, Lgr3 receptor-expressing neurons regulated by damaged disc-derived Dilp8 are known to cause systemic developmental delays via ecdysone signaling in *Drosophila*.[27,28] This is an example of how the CNS affects peripheral tissues, including fat bodies, during injury; however, given that neuronal *TkR86C* knockdown did not induce developmental delay and affected humoral Kyn metabolites (Figures 2C and 4D), TkR86C in neurons would have effects on the regenerative processes themselves rather than developmental processes. Understanding the connections between damaged tissues, fat bodies, and neurons from the viewpoint of TkR86C neurons and Kyn metabolism will provide us with unidentified insights into the systemic regulation of tissue repair.

Limitations of the study

Although we found that neuronal TkR86C was required for disc repair, changes in *TkR86C* expression were not detected in the CNS during disc repair. Given the small number of neurons that co-express *C10-Gal4* and *TkR86C-T2A-LexA*, it is necessary to identify the neurons that contribute to regeneration at the cellular level. Additionally, we did not clarify how *TkR86C*-expressing neurons affect Kyn metabolism. To determine which signals affect Kyn metabolism in the fat body, we will search for factors in *TkR86C*-expressing neurons that regulate Kyn metabolism in the fat body. For example, *TkR86C* neuron-specific proximity labeling of humoral proteins may be useful in identifying proteins that link the CNS to fat bodies. In addition, unlike Tk, NTL could not be functionally analyzed by antibody staining or genetics in this study, and further experiments are required to determine the contribution of NTL. Furthermore, the targets of KynA are yet to be identified. Biochemical methodologies, including receptor screening, are required to determine the role of KynA in disc repair.

STAR★METHODS

Detailed methods are provided in the online version of this paper and include the following:

- KEY RESOURCES TABLE

SUPPLEMENTAL INFORMATION

Supplemental information can be found online at https://doi.org/10.1016/j.isci.2023.107553.

ACKNOWLEDGMENTS

We thank the Bloomington *Drosophila* Stock Center and the Vienna *Drosophila* Resource Center for the fly stocks. We thank S. Kondo (Tokyo University of Science) for providing *TkR86C-T2A-Gal4* flies, Y. Rao for the *TkR86C-T2A-LexA* flies, Z. Gong for the anti-Dilp2 antibody, E. Y. Kim for the anti-Tk antibody, and I. Ando for the anti-P1 antibody. The binding assay was supported by N. Suto from the Drug Discovery Initiative, Graduate School of Pharmaceutical Sciences, University of Tokyo, Japan. We thank A. Inoue (Tohoku University) for discussing the GPCR-binding assay. This work was supported by grants from AMED-Project for Elucidating and Controlling Mechanisms of Aging and Longevity to M.M. under grant no. JP21gm5010001. This work was also supported by grants from the Japan Society for the Promotion of Science to M.M. under grant nos. 16H06385, 21H04774, 21K19206 and 23H04766, and to S.K. under grant no. 21K15100. We thank the members of the Miura laboratory for their technical assistance and discussions, especially K. Takenaga for preparing the fly food and N. Shinoda and Y. Nakajima for their helpful discussions and comments.

AUTHOR CONTRIBUTIONS

S.K., S.M., and M.M. designed the experiments and wrote the manuscript. S.K. and M.M. supervised the study. S.M. and S.K. performed the experiments and analyzed the data.

DECLARATION OF INTERESTS

The authors declare no competing or financial interests.

Received: August 23, 2022
Revised: May 15, 2023
Accepted: August 3, 2023
Published: August 7, 2023

REFERENCES

1. Chera, S., Ghila, L., Dobretz, K., Wenger, Y., Bauer, C., Buzgariu, W., Martinou, J.C., and Galliot, B. (2009). Apoptotic cells provide an unexpected source of Wnt3 signaling to drive hydra head regeneration. Dev. Cell *17*, 279–289. https://doi.org/10.1016/j.devcel.2009.07.014.

2. Li, F., Huang, Q., Chen, J., Peng, Y., Roop, D.R., Bedford, J.S., and Li, C.Y. (2010). Apoptotic cells activate the "phoenix rising" pathway to promote wound healing and tissue regeneration. Sci. Signal. *3*, ra13. https://doi.org/10.1126/scisignal.2000634.

3. Huh, J.R., Guo, M., and Hay, B.A. (2004). Compensatory proliferation induced by cell death in the Drosophila wing disc requires activity of the apical cell death caspase Dronc in a nonapoptotic role. Curr. Biol. *14*, 1262–1266. https://doi.org/10.1016/j.cub.2004.06.015.

4. Pérez-Garijo, A., Martín, F.A., and Morata, G. (2004). Caspase inhibition during apoptosis causes abnormal signalling and developmental aberrations in Drosophila. Development. https://doi.org/10.1242/dev.01432.

5. Ryoo, H.D., Gorenc, T., and Steller, H. (2004). Apoptotic cells can induce compensatory cell proliferation through the JNK and the Wingless signaling pathways. Dev. Cell *7*, 491–501. https://doi.org/10.1016/j.devcel.2004.08.019.

6. Farkas, J.E., Freitas, P.D., Bryant, D.M., Whited, J.L., and Monaghan, J.R. (2016). Neuregulin-1 signaling is essential for nerve-dependent axolotl limb regeneration. Development. https://doi.org/10.1242/dev.133363.

7. Makanae, A., Hirata, A., Honjo, Y., Mitogawa, K., and Satoh, A. (2013). Nerve independent limb induction in axolotls. Dev. Biol. *381*, 213–226. https://doi.org/10.1016/j.ydbio.2013.05.010.

8. Johnston, A.P.W., Yuzwa, S.A., Carr, M.J., Mahmud, N., Storer, M.A., Krause, M.P., Jones, K., Paul, S., Kaplan, D.R., and Miller, F.D. (2016). Dedifferentiated Schwann cell precursors secreting paracrine factors are required for regeneration of the mammalian digit tip. Cell Stem Cell *19*, 433–448. https://doi.org/10.1016/j.stem.2016.06.002.

9. Sugiura, T., Wang, H., Barsacchi, R., Simon, A., and Tanaka, E.M. (2016). MARCKS-like protein is an initiating molecule in axolotl appendage regeneration. Nature *531*, 237–240. https://doi.org/10.1038/nature16974.

10. Lee, W.J., and Miura, M. (2014). Mechanisms of systemic wound response in Drosophila. Curr. Top. Dev. Biol. *108*, 153–183. https://doi.org/10.1016/B978-0-12-391498-9.00001-2.

11. Kashio, S., Obata, F., and Miura, M. (2017). How tissue damage MET metabolism: Regulation of the systemic damage response. Fly (Austin) *11*, 27–36. https://doi.org/10.1080/19336934.2016.1221549.

12. Kashio, S., Obata, F., Zhang, L., Katsuyama, T., Chihara, T., and Miura, M. (2016). Tissue nonautonomous effects of fat body methionine metabolism on imaginal disc repair in *Drosophila*. Proc. Natl. Acad. Sci. USA *113*, 1835–1840. https://doi.org/10.1073/pnas.1523681113.

13. Kashio, S., and Miura, M. (2020). Kynurenine metabolism in the fat body non-autonomously regulates imaginal disc repair in Drosophila. iScience. https://doi.org/10.1016/j.isci.2020.101738.

14. Jan, Y.N., Ghysen, A., Christoph, I., Barbel, S., and Jan, L.Y. (1985). Formation of neuronal pathways in the imaginal discs of Drosophila melanogaster. J. Neurosci. *5*, 2453–2464. https://doi.org/10.1523/jneurosci.05-09-02453.1985.

15. Hanlon, C.D., and Andrew, D.J. (2015). Outside-in signaling - A brief review of GPCR signaling with a focus on the Drosophila GPCR family. J. Cell Sci. *128*, 3533–3542. https://doi.org/10.1242/jcs.175158.

16. Kashio, S., Obata, F., and Miura, M. (2014). Interplay of cell proliferation and cell death in Drosophila tissue regeneration. Dev. Growth Differ. *56*, 368–375. https://doi.org/10.1111/dgd.12139.

17. Worley, M.I., Setiawan, L., and Hariharan, I.K. (2012). Regeneration and transdetermination in Drosophila imaginal discs. Annu. Rev. Genet. *46*, 289–310. https://doi.org/10.1146/annurev-genet-110711-155637.

18. Nässel, D.R., Zandawala, M., Kawada, T., and Satake, H. (2019). Tachykinins: Neuropeptides that are ancient, diverse, widespread and functionally pleiotropic. Front. Neurosci. *13*, 1262. https://doi.org/10.3389/fnins.2019.01262.

19. Song, W., Veenstra, J.A., and Perrimon, N. (2014). Control of lipid metabolism by tachykinin in Drosophila. Cell Rep. *9*, 40–47. https://doi.org/10.1016/j.celrep.2014.08.060.

20. Im, S.H., Takle, K., Jo, J., Babcock, D.T., Ma, Z., Xiang, Y., and Galko, M.J. (2015). Tachykinin acts upstream of autocrine Hedgehog signaling during nociceptive sensitization in Drosophila. Elife *4*, e10735. https://doi.org/10.7554/eLife.10735.

21. Asahina, K., Watanabe, K., Duistermars, B.J., Hoopfer, E., González, C.R., Eyjólfsdóttir, E.A., Perona, P., and Anderson, D.J. (2014). Tachykinin-expressing neurons control male-specific aggressive arousal in drosophila. Cell *156*, 221–235. https://doi.org/10.1016/j.cell.2013.11.045.

22. Lee, S.H., Cho, E., Yoon, S.E., Kim, Y., and Kim, E.Y. (2021). Metabolic control of daily locomotor activity mediated by tachykinin in Drosophila. Commun. Biol. *4*, 693–714. https://doi.org/10.1038/s42003-021-02219-6.

23. Kondo, S., Takahashi, T., Yamagata, N., Imanishi, Y., Katow, H., Hiramatsu, S., Lynn, K., Abe, A., Kumaraswamy, A., and Tanimoto, H. (2020). Neurochemical organization of the Drosophila brain visualized by endogenously tagged neurotransmitter receptors. Cell Rep. *30*, 284–297.e5. https://doi.org/10.1016/j.celrep.2019.12.018.

24. Deng, B., Li, Q., Liu, X., Cao, Y., Li, B., Qian, Y., Xu, R., Mao, R., Zhou, E., Zhang, W., et al. (2019). Chemoconnectomics: Mapping chemical transmission in Drosophila. Neuron *101*, 876–893.e4. https://doi.org/10.1016/j.neuron.2019.01.045.

25. Pastor-Pareja, J.C., Wu, M., and Xu, T. (2008). An innate immune response of blood cells to tumors and tissue damage in Drosophila. Dis. Model. Mech. *1*, 144–154. , discussion 153. https://doi.org/10.1242/dmm.000950.

26. Kurucz, É., Márkus, R., Zsámboki, J., Folkl-Medzihradszky, K., Darula, Z., Vilmos, P., Udvardy, A., Krausz, I., Lukacsovich, T., Gateff, E., et al. (2007). Nimrod, a putative phagocytosis receptor with EGF repeats in Drosophila plasmatocytes. Curr. Biol. *17*, 649–654. https://doi.org/10.1016/j.cub.2007.02.041.

27. Colombani, J., Andersen, D.S., Boulan, L., Boone, E., Romero, N., Virolle, V., Texada, M., and Léopold, P. (2015). Drosophila Lgr3 couples organ growth with maturation and ensures developmental stability. Curr. Biol. *25*, 2723–2729. https://doi.org/10.1016/j.cub.2015.09.020.

28. Garelli, A., Heredia, F., Casimiro, A.P., Macedo, A., Nunes, C., Garcez, M., Dias, A.R.M., Volonte, Y.A., Uhlmann, T., Caparros, E., et al. (2015). Dilp8 requires the neuronal relaxin receptor Lgr3 to couple growth to developmental timing. Nat. Commun. *6*, 8732. https://doi.org/10.1038/ncomms9732.

29. Jakutis, G., and Stainier, D.Y.R. (2021). Genotype-phenotype relationships in the context of transcriptional adaptation and genetic robustness. Annu. Rev. Genet. *55*, 71–91. https://doi.org/10.1146/annurev-genet-071719-020342.

30. Jiang, H., Lkhagva, A., Daubnerová, I., Chae, H.S., Simo, L., Jung, S.H., Yoon, Y.K., Lee, N.R., Seong, J.Y., Zitňan, D., et al. (2013). Natalisin, a tachykinin-like signaling system, regulates sexual activity and fecundity in insects. Proc. Natl. Acad. Sci. USA *110*, E3526–E3534. https://doi.org/10.1073/pnas.1310676110.

31. Poels, J., Birse, R.T., Nachman, R.J., Fichna, J., Janecka, A., Vanden Broeck, J., and Nässel, D.R. (2009). Characterization and distribution of NKD, a receptor for Drosophila tachykinin-related peptide 6. Peptides (N.Y.) *30*, 545–556. https://doi.org/10.1016/j.peptides.2008.10.012.

32. Birse, R.T., Söderberg, J.A.E., Luo, J., Winther, Å.M.E., and Nässel, D.R. (2011). Regulation of insulin-producing cells in the adult Drosophila brain via the tachykinin peptide receptor DTKR. J. Exp. Biol. *214*, 4201–4208. https://doi.org/10.1242/jeb.062091.

33. MacKenzie, A.E., Lappin, J.E., Taylor, D.L., Nicklin, S.A., and Milligan, G. (2011). GPR35 as a novel therapeutic target. Front. Endocrinol. *2*, 68. https://doi.org/10.3389/fendo.2011.00068.

34. Inoue, A., Raimondi, F., Kadji, F.M.N., Singh, G., Kishi, T., Uwamizu, A., Ono, Y., Shinjo, Y., Ishida, S., Arang, N., et al. (2019). Illuminating G-protein-coupling selectivity of GPCRs. Cell *177*, 1933–1947.e25. https://doi.org/10.1016/j.cell.2019.04.044.

35. Koto, A., Motoyama, N., Tahara, H., McGregor, S., Moriyama, M., Okabe, T., Miura, M., and Keller, L. (2019). Oxytocin/vasopressin-like peptide inotocin regulates cuticular hydrocarbon synthesis and water balancing in ants. Proc. Natl. Acad. Sci. USA *116*, 5597–5606. https://doi.org/10.1073/pnas.1817788116.

36. Satoh, A., Graham, G.M.C., Bryant, S.V., and Gardiner, D.M. (2008). Neurotrophic regulation of epidermal dedifferentiation during wound healing and limb regeneration in the axolotl (Ambystoma mexicanum). Dev. Biol. *319*, 321–335. https://doi.org/10.1016/j.ydbio.2008.04.030.

37. Izumi, T., Imai, J., Yamamoto, J., Kawana, Y., Endo, A., Sugawara, H., Kohata, M., Asai, Y., Takahashi, K., Kodama, S., et al. (2018). Vagus-macrophage-hepatocyte link promotes post-injury liver regeneration and whole-body survival through hepatic FoxM1 activation. Nat. Commun. *9*, 5300–5313. https://doi.org/10.1038/s41467-018-07747-0.

38. Suvas, S. (2017). Role of substance P neuropeptide in inflammation, wound healing, and tissue homeostasis. J. Immunol. *199*, 1543–1552. https://doi.org/10.4049/jimmunol.1601751.

39. Kim, D.J., Moon, J.Y., Kim, S.M., Seo, J.W., Lee, Y.H., Jung, S.W., Kim, K., Kim, Y.G., Lim, S.J., Lee, S., et al. (2020). Substance P improves renal ischemia reperfusion injury through modulating immune response. Front. Immunol. *11*, 600–614. https://doi.org/10.3389/fimmu.2020.00600.

40. Steinhoff, M.S., von Mentzer, B., Geppetti, P., Pothoulakis, C., and Bunnett, N.W. (2014). Tachykinins and their receptors: Contributions to physiological control and the mechanisms of disease. Physiol. Rev. *94*, 265–301. https://doi.org/10.1152/physrev.00031.2013.

41. Perner, C., Flayer, C.H., Zhu, X., Aderhold, P.A., Dewan, Z.N.A., Voisin, T., Camire, R.B., Chow, O.A., Chiu, I.M., and Sokol, C.L. (2020). Substance P release by sensory neurons triggers dendritic cell migration and initiates the type-2 immune response to allergens. Immunity *53*, 1063–1077.e7. https://doi.org/10.1016/j.immuni.2020.10.001.

42. Trevisani, M., Siemens, J., Materazzi, S., Bautista, D.M., Nassini, R., Campi, B., Imamachi, N., Andrè, E., Patacchini, R., Cottrell, G.S., et al. (2007). 4-Hydroxynonenal, an endogenous aldehyde, causes pain and neurogenic inflammation through activation of the irritant receptor TRPA1. Proc. Natl. Acad. Sci. USA *104*, 13519–13524. https://doi.org/10.1073/pnas.0705923104.

43. Garay, E., Schuth, N., Barbanente, A., Tejeda-Guzm, C., Vitone, D., Osorio, B., Clark, A.H., Nachtegaal, M., Haumann, M., Dau, H., et al. (2022). Tryptophan regulates Drosophila zinc stores. Proc. Natl. Acad. Sci. USA. https://doi.org/10.1073/pnas.2117807119.

44. Tang, H.B., Miyano, K., and Nakata, Y. (2009). Modulation of the substance P release from cultured rat primary afferent neurons by zinc ions. J. Pharmacol. Sci. *110*, 397–400. https://doi.org/10.1254/jphs.09033SC.

45. Blomeley, C., and Bracci, E. (2008). Substance P depolarizes striatal projection neurons and facilitates their glutamatergic inputs. J. Physiol. *586*, 2143–2155. https://doi.org/10.1113/jphysiol.2007.148965.

46. Agudelo, L.Z., Femenía, T., Orhan, F., Porsmyr-Palmertz, M., Goiny, M., Martinez-Redondo, V., Correia, J.C., Izadi, M., Bhat, M., Schuppe-Koistinen, I., et al. (2014). Skeletal muscle PGC-1α1 modulates kynurenine metabolism and mediates resilience to stress-induced depression. Cell *159*, 33–45. https://doi.org/10.1016/j.cell.2014.07.051.

47. Agudelo, L.Z., Ferreira, D.M.S., Cervenka, I., Bryzgalova, G., Dadvar, S., Jannig, P.R., Pettersson-Klein, A.T., Lakshmikanth, T., Sustarsic, E.G., Porsmyr-Palmertz, M., et al. (2018). Kynurenic acid and Gpr35 regulate adipose tissue energy homeostasis and inflammation. Cell Metab. *27*, 378–392.e5. https://doi.org/10.1016/j.cmet.2018.01.004.

48. Torosyan, R., Huang, S., Bommi, P.V., Tiwari, R., An, S.Y., Schonfeld, M., Rajendran, G., Kavanaugh, M.A., Gibbs, B., Truax, A.D., et al. (2021). Report hypoxic preconditioning protects against ischemic kidney injury through the IDO1/kynurenine pathway ll hypoxic preconditioning protects against ischemic kidney injury through the IDO1/kynurenine pathway. Cell Rep. *36*, 109547. https://doi.org/10.1016/j.celrep.2021.109547.

49. Cervenka, I., Agudelo, L.Z., and Ruas, J.L. (2017). Kynurenines: Tryptophan's metabolites in exercise, inflammation, and mental health. Science *357*, eaaf9794. https://doi.org/10.1126/science.aaf9794.

50. Rossi, A., Kontarakis, Z., Gerri, C., Nolte, H., Hölper, S., Krüger, M., and Stainier, D.Y.R. (2015). Genetic compensation induced by deleterious mutations but not gene knockdowns. Nature *524*, 230–233. https://doi.org/10.1038/nature14580.

51. Okamoto, N., and Watanabe, A. (2022). Interorgan communication through peripherally derived peptide hormones in Drosophila. Fly (Austin) *16*, 152–176. https://doi.org/10.1080/19336934.2022.2061834.

52. Rajan, A., and Perrimon, N. (2012). Drosophila cytokine unpaired 2 regulates physiological homeostasis by remotely controlling insulin secretion. Cell *151*, 123–137. https://doi.org/10.1016/j.cell.2012.08.019.

53. Agrawal, N., Delanoue, R., Mauri, A., Basco, D., Pasco, M., Thorens, B., and Léopold, P. (2016). The Drosophila TNF eiger is an adipokine that acts on insulin-producing cells to mediate nutrient response. Cell Metab. *23*, 675–684. https://doi.org/10.1016/j.cmet.2016.03.003.

54. Li, Q., and Gong, Z. (2015). Cold-sensing regulates Drosophila growth through insulin-producing cells. Nat. Commun. *6*, 10083. https://doi.org/10.1038/ncomms10083.

55. Kennerdell, J.R., and Carthew, R.W. (2000). Heritable gene silencing in Drosophila using double-stranded RNA. Nat. Biotechnol. *18*, 896–898. https://doi.org/10.1038/78531.

56. Guo, G., Yang, J., Nichols, J., Hall, J.S., Eyres, I., Mansfield, W., and Smith, A. (2009). Klf4 reverts developmentally programmed restriction of ground state pluripotency. Development *136*, 1063–1069. https://doi.org/10.1242/dev.030957.

STAR★METHODS

KEY RESOURCES TABLE

REAGENT or RESOURCE	SOURCE	IDENTIFIER
Antibodies		
Mouse anti-Wg	Developmental Studies Hybridoma Bank	Cat#4D4; RRID: AB_528512
Rat anti-GFP (GF090R)	nacalai tesque	Cat#04404-26; RRID: AB_2314545
Rabbit anti-mCherry	Abcam	Cat#ab167453; RRID: AB_2571870
Mouse anti-hemocyte P1	Gift from I. Ando[26]	N/A
Guinea pig anti-Tk	Gift from E. Y. Kim[22]	N/A
Rabbit anti-Dilp2	Gift from Z. Gong[54]	N/A
Anti–mouse IgG, 488	Thermo Fisher Science	Cat#A-21202; RRID: AB_141607
Anti-rat IgG, 488	Thermo Fisher Science	Cat#A-21208; RRID: AB_2535794
Anti-mouse-IgG, 647	Thermo Fisher Science	Cat#A-31571; RRID: AB_162542
Anti-rabbit-IgG, 647	Thermo Fisher Science	Cat#A-31573; RRID: AB_2536183
Anti-mouse-IgG, Cy3	Jackson Immuno Research	Cat#712-166-151; RRID: AB_2340817
Anti-rabbit-IgG, Cy3	Jackson Immuno Research	Cat#711-165-152; RRID: AB_2307443
Chemicals, peptides, and recombinant proteins		
Hoechst33342	Invitrogen	Cat#H3570
Fluoromount-G™	Southern Biotech	Cat#00-4958-02
Kynurenic acid	Sigma-Aldrich	Cat#K3375
NTL-5: LQLRDLYNADDPFVPNR-amidation	Biologica	N/A
Tk-6: pyroglutamate-QRFADFNSKFVAVR-amidation	Biologica	N/A
Experimental models: Organisms/strains		
D. melanogaster: QUAS-DtA^{ts}	Kashio et al.[12]	N/A
D. melanogaster:WP-QF2	Kashio et al.[12]	N/A
D. melanogaster:C10-Gal4	Gift from E. Hafen	N/A
D. melanogaster:UAS-lacZ-RNAi	Gift from R. W. Carthew[54]	N/A
D. melanogaster:UAS-lacZ	Gift from C. Goodman	N/A
D. melanogaster:TkR86C-T2A-Gal4	Gift form S. Kondo[23]	N/A
D. melanogaster:TkR86C-T2A-lexA	Gift from Y. Rao[24]	N/A
D. melanogaster:UAS-rpr	BDSC	#5824
D. melanogaster:UAS-GFP	BDSC	#1521
D. melanogaster:rn-Gal4	BDSC	#51280
D. melanogaster:nSyb-Gal4	BDSC	#51635
D. melanogaster:QUAS-mCD8-GFP	BDSC	#30002
D. melanogaster:QUAS-mCD8-GFP	BDSC	#30003
D. melanogaster:UAS-nls-mCherry	BDSC	#38425
D. melanogaster:UAS-mCD8-ChRFP	BDSC	#27391
D. melanogaster:UAS-mCD8-ChRFP	BDSC	#27392
D. melanogaster:LexAop-mCD8-GFP	BDSC	#32203
D. melanogaster:LexAop-nls-GFP	BDSC	#29954
D. melanogaster:Tk-T2A-Gal4	BDSC	#84693
D. melanogaster:UAS-Tk-RNAi	BDSC	#25800
D. melanogaster:UAS-TkR86C-RNAi 1	VDRC	v107090

(*Continued on next page*)

Continued

REAGENT or RESOURCE	SOURCE	IDENTIFIER
D. melanogaster:UAS-TkR86C-RNAi 2	VDRC	v13392
Oligonucleotides		
Primers for RT-qPCR, see Table S3	This paper	N/A
Software and algorithms		
ImageJ/FIJI ver 2.9.0	ImageJ/FIJI	RRID: SCR_002285
GraphPad Prism 9.5.1	GraphPad Software	RRID: SCR_002798
Other		
TCS-SP8 confocal microscope	Leica	RRID: SCR_018169
Leica DC 300 FX microscope	Leica	N/A
Leica DMI4000B	Leica	N/A
LCMS 8060	SHIMADZU	N/A
QuantStudio 6 Real-Time PCR system	Thermo Fisher	RRID:SCR_020239
FDSS7000	Hamamatsu Photonics	N/A

RESOURCE AVAILABILITY

Lead contact

Masayuki Miura (miura@mol.f.u-tokyo.ac.jp).

Materials availability

Materials and protocols used in this study are available from the authors upon request.

Data and code availability

- All data reported in this paper will be shared by the lead contact upon request.
- This paper does not report original code.
- Any additional information required to reanalyze the data reported in this paper is available from the lead contact upon request.

EXPERIMENTAL MODEL AND STUDY PARTICIPANT DETAILS

Fly stocks and transgenes

QUAS-DtA^{ts},[12] *WP-QF2*,[12] *C10-Gal4* (gifted by E. Hafen), *UAS-lacZ-RNAi*,[55] and *UAS-lacZ* (gifted by C. Goodman) have been characterized in previous studies. *TkR86C-T2A-Gal4* was gifted by S. Kondo.[23] *TkR86C-T2A-lexA* was a gift from Rao.[24] *UAS-rpr* (#5824), *UAS-GFP* (#1521), *rn-Gal4* (#51280), *nSyb-Gal4* (#51635), *QUAS-mCD8-GFP* (#30002, #30003), *UAS-nls-mCherry* (#38425), *UAS-mCD8-ChRFP* (#27391), *UAS-mCD8-ChRFP* (#27392), *LexAop-nls-GFP* (#29954), *LexAop-mCD8-GFP* (#32203), *UAS-Tk-RNAi* (#25800), and *Tk-T2A-Gal4* (#84693) were obtained from the Bloomington *Drosophila* Stock Center. *UAS-TkR86C-RNAi 1* (v107090), *UAS-TkR86C-RNAi 2* (v13392), and RNAi lines used for GPCR screening (Table S1) were obtained from the Vienna *Drosophila* Resource Center.

METHOD DETAILS

Temperature shift protocol for temporal ablation

Embryos were laid at 25°C for 4 h and were incubated then at 25°C for 24 h after initiation. The starting time point of the embryo laid was defined as after egg laying (AEL) at 0 h. For ablation with *WP-QF2>DtA^{ts}*, basically, flies were raised at 29°C for 54 h from 24 h AEL and shifted to 18°C for 48 h. As for ablation combined with *rn-Gal4*, severe wing phenotype was observed even in the control. Therefore, flies were raised at 29°C for 54 h from 24 h AEL and shifted to 18°C for 38 h. For ablation combined with *TkR86C* mutant, flies were raised at 29°C for 54 h from 24 h AEL and shifted to 18°C for 60 h. Larvae were returned to 29°C after temporal ablation at 18°C. Larvae were either allowed to pupate and eclose or dissected at AA0, 12, and 24. Sex differences in larvae were not considered.

Wing size assessment

We observed wing phenotypes by microscopy and manually classified wing size into three categories for GPCR screening (see GPCR screening) and four categories for other experiments: intact wings, group A; chipped or crumpled wings, group B; wings with a size <50% of control, group D; and wings with phenotypes intermediate between groups B and D, group C. Wing size was counted separately for each sex of fly, but this was not reflected in the graph. The age of the flies was not considered. For representative wing images, flies were preserved in a mixture of ethanol/glycerin (3:1). The adult wings were mounted using Fluoromount-G (Southern Biotech) after dissection in phosphate-buffered saline (PBS). Images were captured using a Leica DC 300 FX microscope (Leica, Wetzlar, Germany).

GPCR screening

In *Drosophila*, 111 genes were identified as GPCR-coding genes (FlyBase), and 106 genes were knocked down in our screening. One or two RNA interference (RNAi) lines were used for each gene. We observed wing phenotypes by microscopy and manually classified wing sizes into three categories: intact wings, group A; wings with a size <50% of control, group C; and wings with phenotypes intermediate between groups A and C, group B. The GPCR genes, which resulted in less than 40% of group A and more than 20% of group C, were candidate receptors.

Immunohistochemistry

Larval tissues were dissected at the indicated time points (AA0, 12, or 24) in PBS, fixed in 4% paraformaldehyde in PBS, and washed with 0.1% Triton X-100 in PBS. The antibodies, probes, and dilutions used are indicated in key resources table. Confocal images were acquired using Leica SP8. Quantification of the Tk signal in the cell body of the larval brain and thoracic VNC and quantification of cell number of *Tk-T2A-Gal4> nls-mCherry* expressing cells in the CNS were performed using Fiji software.

Quantitative RT-PCR

For quantitative RT-PCR (qRT-PCR), total RNA was extracted from five larval fat bodies and four whole larvae using a ReliaPrep RNA Tissue Miniprep System (Promega). Total RNA from larval fat bodies (100 ng) and whole larvae (400ng) was used for cDNA synthesis using a PrimeScript RT Reagent Kit with gDNA Eraser (TAKARA). Quantitative PCR was performed using TAKARA TB Green Premix Ex Taq II (Tli RNase H Plus) and a QuantStudio 6 Real-Time PCR system (Thermo Fisher). *RNA polII* was used as the internal control. The primer sequences were listed in key resources table.

Generation of *TkR86C* knock-out mutant fly using CRISPR/Cas9 system

CRISPR/Cas9 genome editing was used to create a *TkR86C* mutant that lacks the first exon containing the start codon of TkR86C. Double-strand breaks were caused by the sgRNA-Cas9 protein at two locations flanking the first exon. Therefore, upon homologous recombination repair of the break site, a DNA sequence with the fluorescent marker protein DsRed was inserted instead, containing two break sites: a sequence of approximately 200 bases (homology arm) and a sequence of DsRed in between were incorporated into the donor vector pBac. The donor and sgRNA expression vectors were injected into transgenic lines expressing the Cas9 protein under the control of the Act5C promoter, and *TkR86C* mutants were selected using DsRed expression as an indicator.

Pairs of guide RNAs were identified using CRISPR Optimal Target Finder tool available on flyCRISPR (http://flycrispr.molbio.wisc.edu/).

The DNA fragments for the guide RNAs were subcloned using the DNA Ligation Kit (TAKARA) into the BbsI-digested U6b-sgRNA-short vector (a gift from N. Perrimon). The primers were annealed to generate DNA fragments for guide RNAs.

	Forward (5′∼3′)	Reverse (5′∼3′)
Target 1	TTCGGCAGTCTGTAATCAGGATAG	AAACCTATCCTGATTACAGACTGC
Target 2	TTCGGTGGAGTCGAAGTACCTGGA	AAACTCCAGGTACTTCGACTCCAC

To generate the homology-directed repair template, DNA fragments of the 5′ homology arm were assembled into the BsaI site, and the DNA fragment of the 3′ homology arm was assembled into the *Bsa*I site of pBac[3xP3-DsRed_polyA_Scarless_TK] (generated by T. Katsuyama) using NEBuilder HiFi DNA Assembly (New England Biolabs) or In-Fusion HD Cloning (TAKARA).

The PAM sequences of the gRNA-binding sites in the donor template were mutated to prevent Cas9-directed cleavage following the homology-directed repair. The DNA fragments were amplified using PCR using the following primers:

	Forward (5′∼3′)	Reverse (5′∼3′)
5′ Homology Arm	TGAAGGTCTCCTTAATGCATG TGGCTGACAGTTCA	TCTTTCTAGGGTTAAGCAGTCT GTAATCAGGATAGATGGTGGTTT CCGTAATGAT
3′ Homology Arm	TCTTTCTAGGGTTAACATTCC AGGTACTTCGACTC	ATTGACGGCTCTTCAAAGT GCATCGACTTAACCGG

The detailed plasmid DNA sequences are available upon request. Transgenic flies were generated by BestGene, Inc. Each DsRed-positive transformant was isogenized and confirmed using genomic PCR and sequencing.

KynA-feeding experiments

Kynurenic acid (Sigma-Aldrich) was diluted with 0.1 N NaOH, and 80 mM stocks were maintained at −80 °C. A volume of 12.5 μL of 80 mM stock was added to 2 mL of fly food to make 0.5 mM KynA food. The larvae were transferred to KynA food 0 h after ablation (AA0).

Generation of a stable cell line for GPCR-binding assay

The methods used for the GPCR-binding assay were based on a previous study.[35] The TkR86C-V5-mCherry fragment was infused into the PB-Gα15-FLAG-IRES-puroR vector (provided by A. Koto) and digested with *Age*I and *Bam*HI (Takara Bio). HEK293T cells were cultured in DMEM (10% FBS and 1% penicillin/streptomycin) at 37°C, 5% CO_2. pPB-TkR86C-mCherry, pPB-Gα15-FLAG-IRES-puroR, and the PiggyBac transposase vector (pCAGGS-PBase)[56] were mixed in the following ratio (45:45:10, total 4 μg) and transfected into HEK293T cells using Lipofectamine 2000 (Thermo Fisher Scientific), following the manufacturer's instructions. Transfected cells were selected using 1 μM puromycin (Sigma-Aldrich) and 400 μg/mL neomycin G418 (Sigma-Aldrich). Individual cell colonies were picked and separated using 0.05% trypsin-EDTA (Thermo Fisher Scientific) and cultured in 6-well dishes in DMEM. Stable cell lines were selected based on the mCherry signal (excitation; 515–560 nm, emission, >590 nm) using a fluorescence microscope (Leica DMI4000B).

Cell preparation for the calcium assay

Cultured cells were washed with PBS and trypsinized with 1 mL 0.05% trypsin-EDTA. To load the fluorescent probe into the cells, the PBS-washed cell pellet was resuspended in 2 mL of loading buffer with 1μM Fluo-4 AM (Dojindo), 0.04% Pluronic F-127 (Sigma-Aldrich), 2.5 mM Probenecid (Thermo Fisher Scientific), and 20 mM HEPES (Thermo Fisher Scientific) in HBSS (Thermo Fisher Scientific). The cell suspension was incubated for 30 min at 37°C under light shielding conditions. After centrifugation and removal of the supernatant, the precipitate was resuspended in 8 mL of recording buffer (2.5 mM probenecid and 20 mM HEPES in HBSS). The cells were dispensed at 20 μL/well using a Multidrop Combi (Thermo Fisher Scientific) into a 384-well assay plate (Greiner) in which 100 nL of 1 mM compound solution was dispensed in advance. After 1 h of incubation at 37°C with light shielding, a calcium assay was performed.

GPCR-binding assay

A Functional Drug Screening System (FDSS7000; Hamamatsu Photonics) was used to measure the fluorescence level of Fluo-4, with excitation and emission wavelength bands centered at 480 and 540 nm, respectively. The ligand was diluted with a buffer (20 mM HEPES in HBSS) and dispensed into a non-binding 384-well plate (Greiner). A total of 5 μL of ligand solution was dispensed into each well with a plastic tip (Hamamatsu Photonics) 10 s after the start of the measurement. The fluorescence intensity was measured

for 2 min on each plate. The average fluorescence intensity from 1 to 10 s was used as the basal, and the maximum fluorescence intensity from 11 to 120 s was used as the peak in the measurement. The response was measured as follows: Response = (Peak-Basal)/Basal. The NTL-5 and Tk-6 peptides for the GPCR-binding assay were produced as previously described.[30,31] The following peptides were obtained from Biologica: NTL-5: LQLRDLYNADDPFVPNR-amidation; Tk-6: pyroglutamate-QRFADFNSKFVAVR-amidation.

Metabolites extraction from larval samples

For the extraction of metabolites from larval hemolymph, five larvae were collected at the indicated time points, and the cuticle was ruptured in cooled PBS. The diluted solution was centrifuged at 1,000 × *g*, 4°C for 5 min. The collected supernatant was immediately frozen and stored at −80°C. Methanol, PBS, and chloroform (9:5:10) were added to the samples and shaken. Samples were centrifuged at 2,300 × *g*, 4°C for 5 min. A centrifugal filter (Nanosep with 10 K Omega, Pall Corporation) was prewashed with Milli-Q water. The supernatant was collected, transferred to a prewashed centrifugal filter unit, and centrifuged at 14,000 × *g*, 4°C for 10–30 min. The sample tube contents were evaporated using a centrifugal concentrator CC-105 (TOMY). The pellets were diluted with Milli-Q water. The sample tubes were then stored at −80°C until analysis. For the extraction of metabolites from larval fat bodies, metabolites were extracted in 50% methanol. Samples were deproteinized in 50% acetonitrile and evaporated completely using a centrifugal concentrator CC-105 (TOMY). The pellets were dissolved in Milli-Q water and filtered through a prewashed centrifugal filter (Nanosep with 10 K Omega, Pall Corporation). The sample tubes were then stored at −80°C until analysis. The amount of protein was quantified for normalization. After metabolite extraction, proteins were extracted from the precipitates using methanol and chloroform. The precipitates were washed in acetone, and the protein was extracted with 0.1 N NaOH at 95°C for 5 min. The protein content was measured using a BCA protein assay kit (Thermo Fisher Scientific).

UPLC-MS/MS

The metabolites were measured using ultra-high-performance liquid chromatography equipped with tandem mass spectrometry (UPLC-MS/MS), SHIMAZU 8060. For metabolite analysis, extracted samples were diluted in an equal volume of Milli-Q water. Each sample was injected, and the concentration was calculated based on a standard curve obtained from serial dilutions of the standard solution for each metabolite. Statistical analyses were conducted using GraphPad Prism software.

QUANTIFICATION AND STATISTICAL ANALYSIS

Groups were compared using a one-way analysis of variance (ANOVA). Tukey's multiple comparison test was applied to Figures 4B–4D, S8E, S8F, S9, and S12. The Chi-squared test was applied to Figures 1C, 2A, 3A, 4E, S3, S6B, S6C, and S8A. Two-tailed student's t-test was applied to Figures 3E and S6A. All analyses were performed using GraphPad Prism 9 (GraphPad Software, Inc., CA, USA). All error bars in the figures represent standard error of the mean (SEM). No statistical method was used to determine the sample size. The experiments were neither randomized nor blindly analyzed.